

The supremum principle selects simple, transferable models

Cody Petrie,* Christian Anderson, Casie Maekawa, Travis Maekawa, and Mark K. Transtrum†

*Department of Physics and Astronomy
Brigham Young University
Provo, UT 84602*

(Dated: February 15, 2022)

We consider how mathematical models enable predictions for conditions that are qualitatively different from the training data. We propose techniques based on information topology to find models that can apply their learning in regimes for which there is no data. The first step is to use the Manifold Boundary Approximation Method to construct simple, reduced models of target phenomena in a data-driven way. We consider the set of all such reduced models and use the topological relationships among them to reason about model selection for new, unobserved phenomena. Given minimal models for several target behaviors, we introduce the *supremum principle* as a criterion for selecting a new, transferable model. The supremal model, i.e., the least upper bound, is the simplest model that reduces to each of the target behaviors. We illustrate how to discover supremal models with several examples; in each case, the supremal model unifies causal mechanisms to transfer successfully to new target domains. These examples culminate in a general algorithm that has formal connections to theories of analogical reasoning in cognitive psychology.

One of the first important tasks in modeling data is selecting the form for a mathematical model. The form of the model defines the types of predictions a model can make and therefore—accurately or not—creates a type of “hypothesis space” called *inductive bias* [1]. In this study, we use the geometric and topological relationships among candidate models to reason about inductive bias and model selection. Of particular interest are predictions for qualitatively different conditions than those on which a model was trained, such as predicting a time series outside of the range of sampled time points, predicting under different experimental conditions, or applying insights from two populations to a third. A model’s ability to make such *out-of-domain* predictions is sometimes known as *transferability*, which is stronger than generalization, i.e., predicting data generated for inputs similar to those on which it was trained [2]. We propose a general principle of model selection, the *supremum principle*, that encodes a preference for simplicity with respect to target quantities of interest while enabling model transferability and whose construction uses topological relationships formally equivalent to models of human analogical reasoning.

A minimal criterion for a useful predictive model is that it reproduces the training data within statistical noise, that is, a kind of coarse interpolation. Common statistical practices such as holdout, jackknife, and cross-validation reinforce this intuition. Sloppy models [3–6], a class of over-parameterized models, further formalize the relation between prediction and interpolation using information geometry [7, 8]. The predictions of sloppy models are controlled by only a few *stiff* parameter combinations and so are said to have a *low effective dimensionality* [8, 9]. Effective dimensionality is quantified in

terms of widths of a model manifold, rigorous bounds for which are given by theorems from interpolation theory [8, 10]. Indeed, it has been suggested that predictive models are generalized interpolation schemes [11].

However, there is a sense that more than simple interpolation ought to be possible [12, 13]. Human cognition is driven by understanding, rather than mere pattern mimicry. When we reason about molecular bonds as if they were balls and springs, we use analogical reasoning to identify abstract relationships and transfer insights among superficially different systems. Can machines similarly analogize to make predictions of a qualitatively different nature than those on which they were trained?

To explore this question, we use information geometry to assess parameter identifiability and predictive performance for models fit to data from different regimes and reason about the hypotheses they encode. The Fisher Information Matrix (FIM) is information geometry’s fundamental object, a Riemannian metric on a manifold of models using parameters as coordinates [8, 14]. Model manifolds are often thin, and boundaries correspond to simplified models, i.e., having fewer parameters [15]. Distances measured by the FIM typically *compress* the model manifold into a few relevant directions [6] so that the manifold is thin and well-approximated by a low-dimensional, simplified model that resides on the boundary. Given training data, the Manifold Boundary Approximation Method (MBAM) explicitly finds limiting approximations to give a minimal, reduced model that encodes the information in the data.

Given several reduced models for target quantities of interest, we next seek a single model that unifies their simplified explanations. To choose an appropriate model, we introduce the *supremum principle*: select the simplest model that is reducible to each of the target behaviors. One of the primary contributions of this paper is to show that this intuitive idea can be given a rigorous definition using the formalism of information topology. We call this

* codypetrie89@gmail.com

† mktranstrum@byu.edu

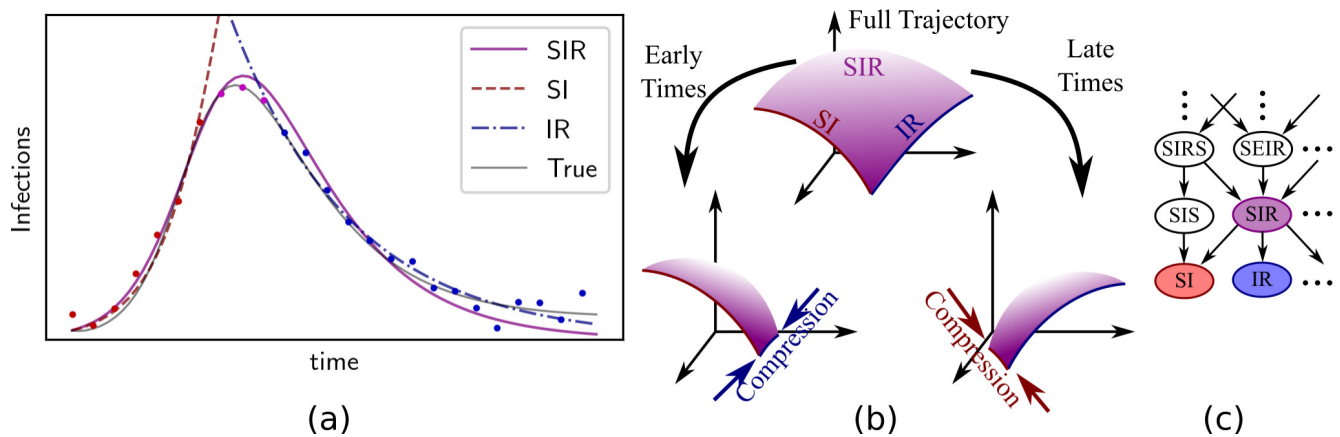


FIG. 1: (a) Infections versus time for a hypothetical epidemic. Data taken at different times—early (red), late (blue), and intermediate (purple)—exhibit qualitatively different types of behaviors. These data carry information about different aspects of the generating process. (b) Information geometry quantifies how data identify a model’s parameters. The full trajectory completely identifies an SIR model, manifest by a model manifold that is not compressed along either direction. Restricting to data at early times compresses the directions related to a recovery rate so that the model is well-approximated by an effective SI model. Similarly, restricting to late times compresses information about infection, leading to an effective IR model. (c) Candidate models of varying complexity can be arranged hierarchically in a directed graph. The SIR model is the *supremum* of the SI and IR models, i.e., the simplest model that combines information from both early and late times. It can use the information from data in two of the regimes to accurately predict a third.

model the *supremal model* and give an algorithm below for constructing it. The supremum principle formally encapsulates a preference for simplicity akin to Occam’s razor, motivated by the assumption that abstract models that explain multiple behaviors are more likely to transfer accurately to novel behaviors than models developed for a single phenomenon.

As a motivating example, consider modeling infection trajectories during an epidemic. Fig. 1a shows data generated from an MSEIR model with birth and death rates (six parameters, fifth-order dynamics) and corrupted by Gaussian noise. We partition the data into three qualitatively distinct regimes—early (red), intermediate (purple), and late (blue)—and ask: Which subsets of the data are informative for predicting data in another regime?

To illustrate the key principles, consider fitting the data with a simple SIR model (two parameters, second-order dynamics),

$$\frac{dS}{dt} = -\beta I \frac{S}{N}, \quad \frac{dI}{dt} = -\gamma I + \beta I \frac{S}{N}, \quad \frac{dR}{dt} = \gamma I. \quad (1)$$

When fitting to qualitatively different data, the two-dimensional SIR model manifold is compressed depending on the informativity of the available data. The compression determines which parameters are identifiable from data and leads to an appropriate reduced model.

We focus on two reduced models on the boundary of the SIR model, shown in Fig. 1b. The first boundary segment, corresponding to $\gamma \rightarrow 0$, is the model with no recovery compartment, i.e., an “SI” model. Similarly, the “IR” model with $\beta \rightarrow \infty$ has a very fast infection

rate. Consider only data from early times (red in Fig. 1). The FIM compresses the model manifold along the SI boundary segment, rendering the recovery rate γ irrelevant. The approximate SI model (red dashed line in Fig. 1) has an effective infection rate that fits the early exponential growth [16]. However, recovery data at later stages (blue), render β irrelevant and are well approximated by the IR model.

The SI and IR models interpolate in their respective domains, but fail to transfer beyond those domains. The SIR model is the simplest that can interpolate all three regimes. Formally, the hierarchy of potential models forms a graded Partially Ordered Set (POSet). A POSet generalizes the concept of order within a set. Real numbers are completely ordered, that is $\forall a, b \in \mathbb{R}$, with $a \neq b$, either $a > b$ or $a < b$. POSets additionally allow for elements to be *incomparable*, i.e., neither $a > b$ nor $a < b$. Discrete POSets can be represented by a directed graph known as a Hasse diagram [24] as in Fig. 1c. In this formalism, the SI and IR models are incomparable; there is no path in the directed graph connecting them. The SIR model is the *supremum* (i.e., least upper bound) of the SI and IR models as it is the simplest model connected to both the SI and IR models within the Hasse diagram. The topological relationships (the adjacency relationships summarized in the Hasse diagram) among candidate models enable reasoning about the mechanisms at play in diverse contexts and inform the construction of the supremal model which minimally merges model elements. The resulting supremal model contains elements not present in either of its children, and so enables predic-

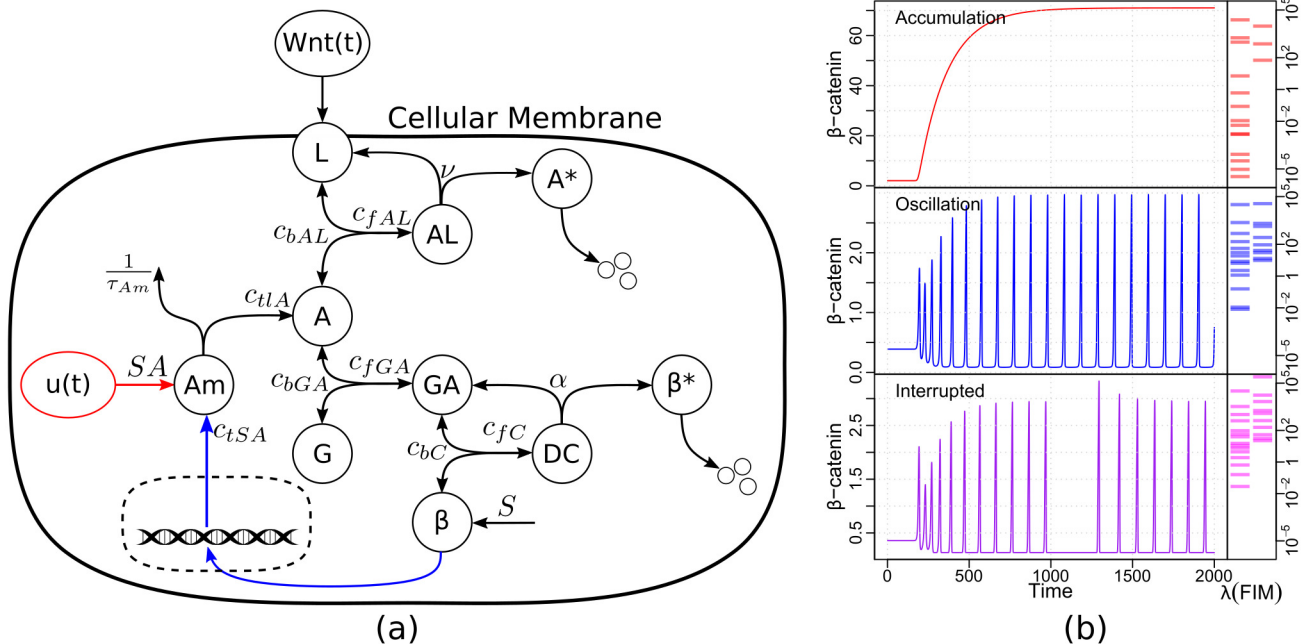


FIG. 2: (a) A network diagram showing the “full” model of the Wnt pathway. The red indicates mechanisms that are unique to the accumulation model, and blue indicates mechanisms unique to the oscillation model. (b) Three possible behaviors of beta-catenin in response to Wnt. The accumulation [17] and oscillation [18] behaviors are known to occur naturally, while behaviors similar to the interrupted behavior have been reported in [19–23].

tions under qualitatively different conditions than either training set.

The supremum principle is applicable to any hierarchical family of models. In this paper, we focus specifically on hierarchies generated by MBAM, which includes things as diverse as power systems [25–28], systems biology [29–32], materials science [33], biogeochemistry [34], nuclear physics [35], neuroscience [36], and others [37–40]. Before giving a general algorithm, we further demonstrate the construction of supremal models in the supplement with a simple network spin model, and in a more complex biological system below.

The Wnt signaling pathway induces cell division in animals, and is one of the best studied in all of biology (See Fig 2a and the Appendix). Via a multi-step process, an extracellular Wnt molecule causes a change in intracellular levels of the transcription factor β -catenin. *In vivo*, β -catenin either “accumulates” to a new, higher equilibrium [17, 41], or “oscillates” between a low baseline and periodic spikes of high concentration [18], as illustrated in Fig. 2b.

To model these two phenomena, we begin with the model proposed by Jensen et al. [18] summarized in Fig 2a. We adapt this model to the accumulation phase by removing the negative feedback loop and replacing it with a controllable activation of Axin2 (as *in vivo* by USP7 [42] among others) denoted by $u(t)$ in Fig. 2. Fig. 2b presents characteristic time series for each of these two models. In each case, the system begins in steady

state and a Wnt stimulus is introduced at 200 minutes. In the first case, β -catenin accumulates and equilibrates at a new steady state [17, 41]. In the second case, the negative feedback loop triggers a Hopf bifurcation leading to sustained oscillations [18].

Each model has 14 parameters. A sloppy model analysis [43, 44] reveals many small eigenvalues (right panel in Fig. 2b) in the respective FIM, indicating that many parameters are unidentifiable. We remove irrelevant parameters using the Manifold Boundary Approximation Method (MBAM) [15], as summarized in Fig. 3a. The accumulation behavior is minimally described by three parameters while the oscillation phenomenon requires nine.

The MBAM reductions are not black boxes. Although the reduced models do abstract away many specific details, they retain vestiges of the full mechanisms, analogous to the SI and IR models in our epidemiology example. To relate these behaviors, we now seek the *supremum* of these two minimal representations. However, unlike the simple example, the minimal Wnt models contain partially overlapping combinations of parameters, so the construction is non-trivial.

Each reduction can be rewritten as a single parameter taken to zero. For example, consider an equilibrium approximation, i.e., $c_f, c_b \rightarrow \infty$. This can be rewritten as a time constant going to zero $\tau_f = 1/c_f \rightarrow 0$ and a nonzero equilibrium constant $K_D = c_b/c_f$. This form, however, is not unique as we could also have chosen $\tau_b = 1/c_b \rightarrow 0$. For all equilibrium approximations we adopt the first as

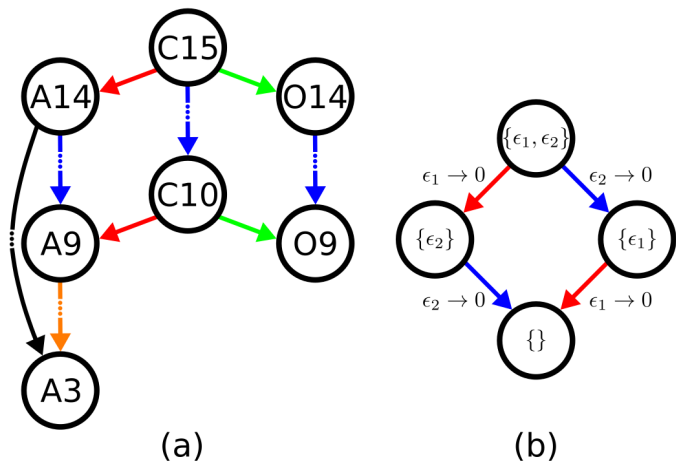


FIG. 3: (a) The Hasse diagram of key reduced models for the Wnt system. The nodes (models) are labeled by “A” for accumulation, “O” for oscillation, “C” for combined, as well as the number of parameters each model contains. The black line represents the original sequence of reduced accumulation models and the blue line represents the new sequence with parameter limits reordered to match those in the oscillation models. The central, blue arrow shows that the original model can be reduced to the supremal model using the same set of limits used to arrive at A9 and O9. Details about the model equations and sequence of limits can be found in the supplemental material. (b) A general example of the diamond property. Consider a model with N parameters containing two parameters ϵ_1 and ϵ_2 . The diamond property states that the order in which parameters can be removed commutes. The same model with $N - 2$ parameters can be reached by first taking either ϵ_1 or ϵ_2 to zero, and then taking the other to zero. The diamond property is used to reorder the limits of a sequence, to build a supremal model.

a standard form.

Next, we observe that the same reduced models could be derived by applying the same approximations in different orders. Commuting the order of reductions creates a diamond motif in the Hasse diagram, as in Fig. 3b. Because of the ambiguity in how reductions are labeled, consecutive limits including the same parameters can obscure this commutation relation. For example, consider the consecutive limits of an equilibrium approximation ($c_{bGA} \rightarrow \infty$, $c_{fGA} \rightarrow \infty$ with c_{bGA}/c_{fGA} constant and finite) followed by an irreversible approximation ($c_{bGA}/c_{fGA} \rightarrow 0$, $c_{fAL} \rightarrow \infty$). Reparameterizing as $\epsilon_1 = 1/c_{fGA}$, $\epsilon_2 = 1/c_{fAL}$, and $\phi = c_{fAL}c_{bGA}/c_{fGA}$ makes the diamond property apparent. The two limits of the diamond property can now be written as $\epsilon_1 \rightarrow 0$ and $\epsilon_2 \rightarrow 0$.

Writing all of the reductions in a standard form allows us to identify the approximations common to both reduced models. Applying these common approximations

to the original full model constructs the supremal model, as illustrated by the blue line connecting C15 to C10 in Fig. 3. This procedure is formalized as a four step algorithm: First, apply MBAM to construct reduced models for the observed target behaviors. Second, put each of the limits in standard form. Third, select the intersection of the sets of limits from each reduction, and fourth, apply those common limits to the full model. The supplemental material presents a second algorithm that exploits a general duality inherent in POSets.

By including both the feedback loop and external control, the supremum enables the accumulation and oscillation phenomena, as well as additional behaviors neither A14 nor O14 can produce. Fig. 2b demonstrates one such example, the “interrupted” behavior, in which the external control modulates the phase of the oscillation. Regular oscillatory behavior in the Wnt pathway is well-known *in vivo* from the segmentation clock in vertebrate embryos along the anterior-posterior axis to establish, for example, the repeating pattern of vertebrae and ribs [45]. These regular oscillations can have their period and phase modified, stopped, or restarted through manipulation of “dorsalizing” or “ventralizing” molecular regulators, much like the interrupted behavior we see in the supremal model [19–23]. To validate our model, we apply MBAM to the head node using the predictions for this novel behavior. This reduction gives the supremal model constructed by our algorithm, indicating that the supremum is the model that would have been selected had observations been available for this behavior.

The supremum principle shows promise for transferring predictability to truly new domains. For example, the SI and IR models fail in the intermediate regime, and the accumulation and oscillation models fail in the interrupted regime, but the supremal models in each case are able to embrace all three behaviors. It does this by including key modeling elements (e.g., feedback and external control) that are missing from the reduced models. Since the supremal model combines distinct modeling elements, it enables new behaviors in regimes in which those modeling elements are all necessary. With a different starting model, couched in a different hypothesis space, the supremal model will be different, but it will still transfer according to the given hypothesis. This is more than the simple generalization of, e.g., multi-task learning (MTL) [46]. Supremal models apply in a more global way; they aim to improve the transferability to data in a completely new regime.

Classical psychological theories use geometric constructions to represent analogical relationships. Most notably, in the parallelogram model [47], an analogy such as man:king::woman:queen is represented as four corners of a parallelogram with analogical relationships forming parallel sides [48]. Such constructions are widespread in AI applications ranging from recommender systems [49] to natural language processing [50]. The key property, however, is the topological relationship between analogous elements [51] that for parallelograms form the same

diamond motif as in Fig. 3. The analogical relationships among words are the same as those between reduced models. Kings are subsets of men just as reduced models are restricted cases of more general models, and classifications based on royalty analogize across genders just as approximations transfer across models. Thus, the supremum construction identifies the mathematical “analogies” between models by teasing out the common mechanisms or analogous reductions (see the colored arrows in Fig. 3). The approximations in linking model C15 to model C10 are the same as those connecting model A14 to model A9, i.e., C15:C10::A14:A9. The colored arrows indicate the many other possible analogies that could be drawn among the models.

The supremum principle is applicable to any hierarchical family of models, and so there are some inherent limitations and potential extensions. First, the algorithm we present here is specific to hierarchies generated by MBAM, but future work could consider other families. Next, the result depends on the hierarchy one uses, for example, our Wnt study used the hierarchy generated by the model of Jensen et al. [18]. Given different hierarchies, supremal models are a principled way of reasoning about the implications of those hypothesis. Future work may use supremal models to guide experimental design for hypothesis testing or parameter estimation. Finally, one could consider models that are derived independently

of a hierarchical family. Future work could explore how to most naturally embed such models within a hierarchy to enable transferability.

Beyond the appeal of elegant, simplified models, we expect supremal models to be of broad practical use; for example, in systems that need a controller to move between two behavioral states, but is difficult to fully model and a reduced model is needed. Such systems include shifting from diseased to healthy states in medical contexts, failing to stable power grids in electrical engineering, ductile to brittle structures in material science, and collapsed to restored resources in ecosystem-based management. Supremal models are also designed for maximal simplicity while retaining some transferability, i.e., attempting to predict in regimes not yet examined, such as in climate modeling, prosperous non-growth-based economics, and human behavior during a pandemic. Practitioners from a wide variety of fields will find supremum modeling a powerful addition to their toolboxes.

This work was supported by the US National Science Foundation under Award NSF-1753357 (CP, CA, MKT), CMMT-1834332 (CP, MKT), and EPCN-1710727 (CA, MKT). We thank Sean Warnick, Kolten Barfuss, and Alex Stankovic for helpful conversations. We thank Ben Francis, Dan Karls, Ellad Tadmor, and Ryan Elliott and two anonymous reviewers for comments on the manuscript.

-
- [1] J. Baxter, *Journal of Artificial Intelligence Research* **12**, 149 (2000).
- [2] K. Weiss, T. M. Khoshgoftaar, and D. Wang, *Journal of Big Data* **3**, 9 (2016).
- [3] K. S. Brown and J. P. Sethna, *Physical Review E* **68**, 021904 (2003).
- [4] K. S. Brown, C. C. Hill, G. A. Calero, C. R. Myers, K. H. Lee, J. P. Sethna, and R. A. Cerione, *Physical Biology* **1**, 184 (2004).
- [5] J. J. Waterfall, F. P. Casey, R. N. Gutenkunst, K. S. Brown, C. R. Myers, P. W. Brouwer, V. Elser, and J. P. Sethna, *Physical Review Letters* **97**, 150601 (2006).
- [6] B. B. Machta, R. Chachra, M. K. Transtrum, and J. P. Sethna, *Science* **342**, 604 (2013).
- [7] S.-i. Amari and H. Nagaoka, *Methods of information geometry*, Vol. 191 (American Mathematical Soc., 2007).
- [8] M. K. Transtrum, B. B. Machta, and J. P. Sethna, *Phys. Rev. Lett.* **104**, 060201 (2010).
- [9] C. H. LaMont and P. A. Wiggins, *Physical Review E* **99**, 052140 (2019).
- [10] K. N. Quinn, H. Wilber, A. Townsend, and J. P. Sethna, *Physical Review Letters* **122**, 158302 (2019).
- [11] M. K. Transtrum, B. B. Machta, and J. P. Sethna, *Physical Review E* **83**, 036701 (2011).
- [12] B. M. Lake, T. D. Ullman, J. B. Tenenbaum, and S. J. Gershman, *Behavioral and Brain Sciences* **40**, e253 (2017).
- [13] T. Webb, Z. Dulberg, S. Frankland, A. Petrov, R. O’Reilly, and J. Cohen, in *Proceedings of the 37th International Conference on Machine Learning*, Proceedings of Machine Learning Research, Vol. 119, edited by H. D. III and A. Singh (PMLR, 2020) pp. 10136–10146.
- [14] A. F. Brouwer and M. C. Eisenberg, arXiv:1802.05641 [math] (2018), arXiv:1802.05641.
- [15] M. K. Transtrum and P. Qiu, *Physical Review Letters* **113**, 098701 (2014).
- [16] Although this approximation is constructed by taking $\gamma \rightarrow 0$, it does not require the “true” value of γ to be small. Rather, the role of the recovery mechanism can be compressed into a simpler model with an effective infection rate, similar to the effective electron mass in a condensed matter system.
- [17] L. Goentoro and M. W. Kirschner, *Molecular Cell* **36**, 872 (2009).
- [18] P. B. Jensen, L. Pedersen, S. Krishna, and M. H. Jensen, *Biophysical Journal* **98**, 943 (2010).
- [19] I. H. Riedel-Kruse, C. Müller, and A. C. Oates, *Science* **317**, 1911 (2007).
- [20] S. Gibb, A. Zagorska, K. Melton, G. Tenin, I. Vacca, P. Trainor, M. Maroto, and J. K. Dale, *Developmental Biology* **330**, 21 (2009).
- [21] A. Goldbeter and O. Pourquié, *Journal of Theoretical Biology* **252**, 574 (2008).
- [22] C. Gomez, E. M. Özbudak, J. Wunderlich, D. Baumann, J. Lewis, and O. Pourquié, *Nature* **454**, 335 (2008).
- [23] Y. Rui, Z. Xu, B. Xiong, Y. Cao, S. Lin, M. Zhang, S. C. Chan, W. Luo, Y. Han, Z. Lu, Z. Ye, H. M. Zhou, J. Han, A. Meng, and S. C. Lin, *Developmental Cell* **13**, 268 (2007).
- [24] M. K. Transtrum, G. Hart, and P. Qiu, *CoRR* (2014),

- arXiv:1409.6203 [physics.data-an].
- [25] V. G. Svenda, M. K. Transtrum, B. L. Francis, A. T. Sarić, and A. M. Stanković, *IEEE Transactions on Power Systems* (2021).
- [26] A. T. Sarić, A. A. Sarić, M. K. Transtrum, and A. M. Stanković, *IEEE Transactions on Power Systems* **36**, 2390 (2020).
- [27] B. L. Francis, J. R. Nuttall, M. K. Transtrum, A. T. Sarić, and A. M. Stanković, in *2019 North American Power Symposium (NAPS)* (IEEE, 2019) pp. 1–6.
- [28] M. K. Transtrum, A. T. Sarić, and A. M. Stanković, *IEEE Transactions on Power Systems* **32**, 2243 (2016).
- [29] J. E. Jeong, Q. Zhuang, M. K. Transtrum, E. Zhou, and P. Qiu, *Quantitative Biology* **6**, 287 (2018).
- [30] M. K. Transtrum and P. Qiu, *PLoS computational biology* **12**, e1004915 (2016).
- [31] B. K. Mannakee, A. P. Ragsdale, M. K. Transtrum, and R. N. Gutenkunst, in *Uncertainty in Biology* (Springer, 2016) pp. 271–299.
- [32] M. K. Transtrum, B. B. Machta, K. S. Brown, B. C. Daniels, C. R. Myers, and J. P. Sethna, *The Journal of chemical physics* **143**, 07B201.1 (2015).
- [33] Y. Kurniawan, C. L. Petrie, K. J. Williams, M. K. Transtrum, E. B. Tadmor, R. S. Elliott, D. S. Karls, and M. Wen, arXiv preprint arXiv:2112.10851 (2021).
- [34] G. L. Marschmann, H. Pagel, P. Kügler, and T. Streck, *Environmental Modelling & Software* **122**, 104518 (2019).
- [35] T. Nikšić, M. Imbrišak, and D. Vretenar, *Physical Review C* **95**, 054304 (2017).
- [36] J. Rasband, *Two Reduced Models of Nerve Behavior*, Bachelor’s thesis, Brigham Young University (2021).
- [37] P. E. Paré, D. Grimsman, A. T. Wilson, M. K. Transtrum, and S. Warnick, *IEEE Transactions on Automatic Control* **64**, 4796 (2019).
- [38] T. Gerach, D. Weiß, O. Dössel, and A. Loewe, in *2019 Computing in Cardiology (CinC)* (IEEE, 2019) p. 1.
- [39] D. M. Lombardo and W.-J. Rappel, *Chaos: An Interdisciplinary Journal of Nonlinear Science* **27**, 093914 (2017).
- [40] P. E. Paré, A. T. Wilson, M. K. Transtrum, and S. C. Warnick, in *2015 American Control Conference* (IEEE, 2015) pp. 1989–1994.
- [41] E. Lee, A. Salic, R. Krüger, R. Heinrich, and M. W. Kirschner, *PLOS Biology* **1**, e10 (2003).
- [42] L. Ji, B. Lu, R. Zamponi, O. Charlat, R. Aversa, Z. Yang, F. Sigoillot, X. Zhu, T. Hu, J. S. Reece-Hoyes, C. Russ, G. Michaud, J. S. Tchorz, X. Jiang, and F. Cong, *Nature Communications* **10**, 4184 (2019).
- [43] R. N. Gutenkunst, J. J. Waterfall, F. P. Casey, K. S. Brown, C. R. Myers, and J. P. Sethna, *PLOS Computational Biology* **3**, e189 (2007).
- [44] M. K. Transtrum, B. B. Machta, and J. P. Sethna, *Physical Review E* **83**, 036701 (2011).
- [45] O. Pourquie, *Science* **301**, 328 (2003).
- [46] R. Caruana, *Machine Learning* **28**, 41 (1997).
- [47] D. E. Rumelhart and A. A. Abrahamson, *Cognitive Psychology* **5**, 1 (1973).
- [48] J. C. Peterson, D. Chen, and T. L. Griffiths, *Cognition* **205**, 104440 (2020).
- [49] C. Musto, in *Proceedings of the fourth ACM conference on Recommender systems* (2010) pp. 361–364.
- [50] J. N. Reid and A. N. Katz, *Metaphor and Symbol* **33**, 280 (2018).
- [51] D. Gentner, *Cognitive Science* **7**, 155 (1983).

SUPPLEMENTARY MATERIAL

S1. SPIN MODEL WITH FERROMAGNETIC COUPLING

Here, we demonstrate the supremum principle with another simple model, a spin model with ferromagnetic coupling as illustrated in the top node of the Hasse diagram in Fig. S1. Spin variables can take on values $s \in \{-1, 0, 1\}$. The model manifold shares the same topology

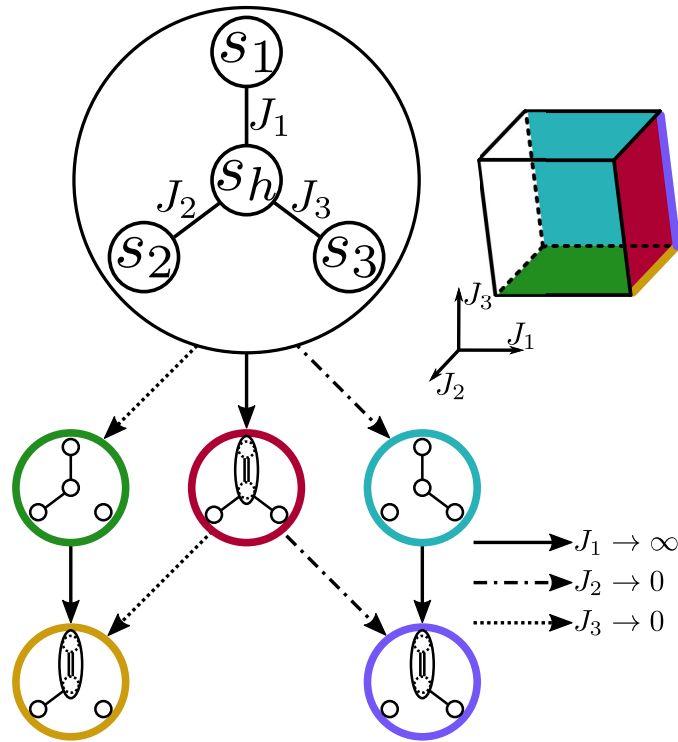


FIG. S1. Hasse diagram showing the POSet of reduced models, including the supremum, for spin model with ferromagnetic coupling on a network. Observables for the left and right flags of Hasse diagram are $P(s_1, s_2)$ and $P(s_1, s_3)$, respectively. The model manifold is diffeomorphic to a cube, which is illustrated in the top right corner. The colored faces and edges represent reduced models, while the red face represents the supremum.

as a cube and is represented in the top right of Fig. S1. The energy function corresponding to the top node in the Hasse diagram of Fig. S1 is

$$H = -J_1 s_1 s_h - J_2 s_2 s_h - J_3 s_3 s_h. \quad (\text{S1})$$

The full probability distribution, marginalized over the hidden spin, is given by

$$P(s_1, s_2, s_3) = \frac{1}{Z} \sum_{s_h=-1,0,1} e^{J_1 s_1 s_h + J_2 s_2 s_h + J_3 s_3 s_h} \quad (\text{S2})$$

$$= \frac{1}{Z} (1 + 2 \cosh(J_1 s_1 + J_2 s_2 + J_3 s_3)), \quad (\text{S3})$$

with the partition function being given by

$$Z = 29 + 4 \cosh(J_3) + 4 \cosh(J_1) (1 + 2 \cosh(J_2)) (1 + 2 \cosh(J_3)) + \cosh(J_2) (4 + 8 \cosh(J_3)). \quad (\text{S4})$$

We consider the case where s_h couples strongly to s_1 but weakly to s_2 and s_3 , and experiments can only measure the correlations $P(s_1, s_2)$ and $P(s_1, s_3)$. The probability for only two spins can be found by marginalizing over one spin and is given by

$$P(s_i, s_j) = \sum_{s_k=-1,0,1} P(s_i, s_j, s_k), \quad (\text{S5})$$

where i and j can be any discrete pair of 1, 2, 3 and k is the remaining spin.

A. Possible MBAM reductions

For ferromagnetic spin systems there are two types of possible reductions that MBAM can find; taking a single J_i to zero or infinity. To illustrate each type of reduction, consider taking J_1 to each of the extreme values for the observable $P(s_1, s_2, s_3)$ in Eq. S3. Taking J_0 to zero is trivial, the two correlated spins are decoupled resulting in the limit

$$\lim_{J_1 \rightarrow 0} P(s_1, s_2, s_3) = \frac{(1 + 2 \cosh(J_2 s_2 + J_3 s_3))}{33 + 12 \cosh(J_2) + 12 \cosh(J_3) + 24 \cosh(J_2) \cosh(J_3)}. \quad (\text{S6})$$

In this case the spins s_1 , s_2 , and s_3 can all take on the values -1 , 0 , and 1 .

The limit $J_1 \rightarrow \infty$ is more subtle. When taking this limit, it is useful to set s_1 to each of its possible values -1 , 0 , and 1 before taking the limit. The reduced model for each probability is given by

$$\lim_{J_1 \rightarrow \infty} P(s_1 = \{-1, 0, 1\}, s_2, s_3) = \frac{\{e^{-J_2 s_2 - J_3 s_3}, 0, e^{J_2 s_2 + J_3 s_3}\}}{2 + 4 \cosh(J_2) + 4 \cosh(J_3) + 8 \cosh(J_2) \cosh(J_3)}. \quad (\text{S7})$$

The configurations with $s_1 = 0$ all have a probability of zero. Thus, this is equivalent to the model

$$\lim_{J_1 \rightarrow \infty} P(s_1, s_2, s_3) = \frac{e^{J_2 s_2 s_1 + J_3 s_3 s_1}}{2 + 4 \cosh(J_2) + 4 \cosh(J_3) + 8 \cosh(J_2) \cosh(J_3)}, \quad (\text{S8})$$

where s_2 and s_3 can be either -1 , 0 , or 1 , but s_1 is restricted to only be -1 or 1 . In this way, reducing the model not only decreases the number of parameters, but also reduces the number of configurations with non-zero probability.

B. Reduced model based on $P(s_1, s_2)$ data

We first consider the case where only s_1 and s_2 can be measured. Observing $P(s_1, s_2)$ renders J_3 practically unidentifiable, represented by the limit $J_3 \rightarrow 0$ and the green face of the model manifold. Further, the strong correlation between s_1 and s_h is represented by the limit $J_1 \rightarrow \infty$ and the gold edge of the model manifold. Applying these limits to $P(s_1, s_2)$ yields the reduced model

$$\lim_{\substack{J_3 \rightarrow 0 \\ J_1 \rightarrow \infty}} P(s_1, s_2) = \frac{e^{J_2 s_2 s_1}}{2 + 4 \cosh(J_2)}. \quad (\text{S9})$$

This is the gold model in the Hasse diagram of Fig. S1 with the energy function

$$H_{\text{gold}} = -J_2 s_2 s_1, \quad (\text{S10})$$

with s_1 confined to be only $-1, 1$, as all configurations with $s_1 = 0$ are zero in this limit.

C. Reduced model based on $P(s_1, s_3)$ data

If we consider the case where only s_1 and s_3 can be measured. By the similar arguments made in the previous section, the relevant limits were $J_2 \rightarrow 0$, $J_1 \rightarrow \infty$. Applying these limits to $P(s_1, s_3)$ yields the reduced model

$$\lim_{\substack{J_2 \rightarrow 0 \\ J_1 \rightarrow \infty}} P(s_1, s_3) = \frac{e^{J_3 s_3 s_1}}{2 + 4 \cosh(J_3)}. \quad (\text{S11})$$

This is the purple model in the Hasse diagram of Fig. S1 with the energy function

$$H_{\text{purple}} = -J_3 s_3 s_1. \quad (\text{S12})$$

Again, s_1 is confined to be only $-1, 1$.

D. Building the supremum

We construct the supremum by applying the overlapping parameter reductions, only $J_1 \rightarrow \infty$ in this simple case, to the original full model. Applying this limit to the full probability function $P(s_1, s_2, s_3)$ yields the supremum:

$$P_{\text{sup}}(s_1, s_2, s_3) = \lim_{J_1 \rightarrow \infty} P(s_1, s_2, s_3) \quad (\text{S13})$$

$$= \frac{e^{J_2 s_2 s_1 + J_3 s_3 s_1}}{Z}, \quad (\text{S14})$$

where the partition function is given by

$$Z = 1 + 4 \cosh(J_2) + 4 \cosh(J_3) + 8 \cosh(J_2) \cosh(J_3). \quad (\text{S15})$$

In this limit s_1 is again restricted to be -1 and 1. This is the supremal model shown in red in Fig. S1, having the energy function

$$H_{\text{sup}} = -J_2 s_2 s_1 - J_3 s_3 s_1, \quad (\text{S16})$$

with $s_1 = -1, 1$ and $s_2, s_3 = -1, 0, 1$. The red face is the lowest dimensional face that contains the gold and purple edges. The supremum contains the information to predict, not only $P(s_1, s_2)$ and $P(s_1, s_3)$, but the experimentally inaccessible distributions, $P(s_2, s_3)$ and $P(s_1, s_2, s_3)$.

S2. WNT SIGNALING PATHWAY

The Wnt signaling pathway is the dominant mechanism for initiating cell division in almost all animals [1]. This relaying of a local signal to the nucleus is crucial to normal embryonic development, stem-cell activation, and cancer tumorigenesis, and thus is one of the best-studied in all of biology. The canonical Wnt pathway is a many-step process, summarized in Fig. 2a. First, one of several extracellular Wnt molecules (such as the eponymous Wingless-or-Int-1 proteins, or one of their many analogues) interacts with two intermembrane proteins: Frizzled and LRP, forming a complex (L). Inside the cell, L binds to Axin (A), thereby removing it from the APC-GSK3-Axin destruction complex (DC) which normally degrades β -catenin (β). In the absence of DC, β -catenin now accumulates and interacts with DNA-associated proteins such as TCF to promote cell division [2, 3] This ‘‘accumulation phenomenon’’ is well-documented in the literature [4, 5] and illustrated in Fig. 2b.

A mass balance model of even this simple outline of the pathway contains over a dozen parameters, obscuring the relationship among output behaviors of β -catenin for different mechanisms. The problem is compounded by the fact that β -catenin is a transcription factor for many different genes depending on the state of the cell. For example, during somitogenesis β -catenin activates Axin2 (a homolog of Axin) leading to a negative feedback loop, driving a limit cycle “oscillation phenomenon” that acts as a segmentation clock [6] (see Fig. 2b).

Various models for the Wnt signaling pathway were discussed in the main text. We will give the equations for each of the most relevant models, i.e., those in Fig. 3a. In the equations, the dynamic equations will be

$$\begin{aligned}
y_1 &= \text{Destruction Complex}[\text{GSK-Axin2-}\beta] \\
y_2 &= [\text{GSK-Axin2}] \\
y_3 &= [\beta - \text{catenin}] \\
y_4 &= [\text{GSK}] \\
y_5 &= [\text{Axin2}] \\
y_6 &= [\text{Axin2}_{\text{mRNA}}] \\
y_7 &= [\text{Axin2-LRP}] \\
y_8 &= [\text{LRP}],
\end{aligned} \tag{S17}$$

where β -catenin is the observed variable in each case, and common renormalized quantities are

$$\begin{aligned}
\tilde{y}_6 &= c_{tLA}y_6 \\
k_{GA} &= c_{bGA}/c_{fGA}.
\end{aligned} \tag{S18}$$

Additionally, the input function for the Wnt and USP7 are given by

$$\begin{aligned}
f_W(t) &= 70.0 \times 0.0398942e^{\frac{-(t-200)^2}{2 \times 10^2}} \\
f_U(t) &= \begin{cases} 15.0e^{\frac{-(t-1050)^2}{2 \times 10^2}}, & \text{Interrupted} \\ 1, & \text{Accumulation,} \end{cases}
\end{aligned} \tag{S19}$$

and time derivatives of the variables are $\dot{y} = dy/dt$.

A14: Accumulation Model, $N = 14$

$$\begin{aligned}
\dot{y}_1 &= c_{fC}y_3y_2 - c_{bC}y_1 - \alpha y_1 \\
\dot{y}_2 &= c_{fGA}y_4y_5 - c_{bGA}y_2 - c_{fC}y_3y_2 + c_{bC}y_1 + \alpha y_1 \\
\dot{y}_3 &= S - c_{fC}y_3y_2 + c_{bC}y_1 \\
\dot{y}_4 &= -c_{fGA}y_4y_5 + c_{bGA}y_2 \\
\dot{y}_5 &= -c_{fGA}y_4y_5 + c_{bGA}y_2 + c_{tIA}y_6 - c_{fAL}y_5y_8 + c_{bAL}y_7 \\
\dot{y}_6 &= -1/\tau_{Am}y_6 + SA \\
\dot{y}_7 &= c_{fAL}y_5y_8 - c_{bAL}y_7 - \nu y_7 \\
\dot{y}_8 &= -c_{fAL}y_5y_8 + c_{bAL}y_7 + \nu y_7 + f_W(t)
\end{aligned} \tag{S20}$$

Conserved Quantities:

$$G_{tot} = y_1 + y_2 + y_4$$

$$L_{tot} = y_7 + y_8$$

A9: Accumulation Model, $N = 9$

$$\begin{aligned}
\dot{y}_2 &= \frac{y_4 (\tilde{y}_6 - c_{fAL}y_5y_8)}{k_{GA} + y_4 + y_5} \\
\dot{y}_3 &= S - c_{fC}y_3y_2 \\
\dot{y}_4 &= -\frac{y_4 (\tilde{y}_6 - c_{fAL}y_5y_8)}{k_{GA} + y_4 + y_5} \\
\dot{y}_5 &= -\frac{y_4 (\tilde{y}_6 - c_{fAL}y_5y_8)}{k_{GA} + y_4 + y_5} + \tilde{y}_6 - c_{fAL}y_5y_8 \\
\dot{\tilde{y}}_6 &= -1/\tau_{Am}\tilde{y}_6 + [SA \cdot c_{tIA}] \\
\dot{y}_7 &= c_{fAL}y_5y_8 - \nu y_7 \\
\dot{y}_8 &= -c_{fAL}y_5y_8 + \nu y_7 + f_W(t)
\end{aligned} \tag{S21}$$

IC conditions:

$$G_{tot} = y_2 + y_4$$

$$L_{tot} = y_7 + y_8$$

A3: Accumulation Model, $N = 3$

$$\dot{y}_3 = S - \theta_1 \frac{y_3}{y_8}$$

$$\dot{y}_8 = f_W(t)$$

Conserved Quantities:

$$y_8 = \theta_2 \tag{S22}$$

Renormalized parameters:

$$\theta_1 = \frac{c_{fC} \cdot c_{fGA} \cdot SA \cdot c_{tLA} \cdot \tau_{Am}}{G_{tot} \cdot c_{fAL} \cdot c_{bGA}}$$

$$\theta_2 = L_{tot} - \frac{SA \cdot c_{tLA} \cdot \tau_{Am}}{\nu}$$

O14: Oscillation Model, $N = 14$

$$\dot{y}_1 = c_{fC}y_3y_2 - c_{bC}y_1 - \alpha y_1$$

$$\dot{y}_2 = c_{fGA}y_4y_5 - c_{bGA}y_2 - c_{fC}y_3y_2 + c_{bC}y_1 + \alpha y_1$$

$$\dot{y}_3 = S - c_{fC}y_3y_2 + c_{bC}y_1$$

$$\dot{y}_4 = -c_{fGA}y_4y_5 + c_{bGA}y_2$$

$$\dot{y}_5 = -c_{fGA}y_4y_5 + c_{bGA}y_2 + c_{tLA}y_6 - c_{fAL}y_5y_8 + c_{bAL}y_7$$

$$\dot{y}_6 = -1/\tau_{Am}y_6 + c_{tsA}y_3^2 \tag{S23}$$

$$\dot{y}_7 = c_{fAL}y_5y_8 - c_{bAL}y_7 - \nu y_7$$

$$\dot{y}_8 = -c_{fAL}y_5y_8 + c_{bAL}y_7 + \nu y_7 + f_W(t)$$

Conserved Quantities:

$$G_{tot} = y_1 + y_2 + y_4$$

$$L_{tot} = y_7 + y_8$$

O9: Oscillation Model, $N = 9$

$$\begin{aligned}
\dot{y}_2 &= \frac{y_4 (\tilde{y}_6 - c_{fAL} y_5 y_8)}{k_{GA} + y_4 + y_5} \\
\dot{y}_3 &= S - c_{fC} y_3 y_2 \\
\dot{y}_4 &= -\frac{y_4 (\tilde{y}_6 - c_{fAL} y_5 y_8)}{k_{GA} + y_4 + y_5} \\
\dot{y}_5 &= -\frac{y_4 (\tilde{y}_6 - c_{fAL} y_5 y_8)}{k_{GA} + y_4 + y_5} + \tilde{y}_6 - c_{fAL} y_5 y_8 \\
\dot{\tilde{y}}_6 &= -1/\tau_{Am} \tilde{y}_6 + [c_{tsA} \cdot c_{tlA}] y_3^2 \\
\dot{y}_7 &= c_{fAL} y_5 y_8 - \nu y_7 \\
\dot{y}_8 &= -c_{fAL} y_5 y_8 + \nu y_7 + f_W(t)
\end{aligned} \tag{S24}$$

Conserved Quantities:

$$G_{tot} = y_2 + y_4$$

$$L_{tot} = y_7 + y_8$$

C15: Combined Model, $N = 15$

$$\begin{aligned}
\dot{y}_1 &= c_{fC} y_3 y_2 - c_{bC} y_1 - \alpha y_1 \\
\dot{y}_2 &= c_{fGA} y_4 y_5 - c_{bGA} y_2 - c_{fC} y_3 y_2 + c_{bC} y_1 + \alpha y_1 \\
\dot{y}_3 &= S - c_{fC} y_3 y_2 + c_{bC} y_1 \\
\dot{y}_4 &= -c_{fGA} y_4 y_5 + c_{bGA} y_2 \\
\dot{y}_5 &= -c_{fGA} y_4 y_5 + c_{bGA} y_2 + c_{tlA} y_6 - c_{fAL} y_5 y_8 + c_{bAL} y_7 \\
\dot{y}_6 &= -1/\tau_{Am} y_6 + c_{tsA} y_3^2 + S A f_U(t) \\
\dot{y}_7 &= c_{fAL} y_5 y_8 - c_{bAL} y_7 - \nu y_7 \\
\dot{y}_8 &= -c_{fAL} y_5 y_8 + c_{bAL} y_7 + \nu y_7 + f_W(t)
\end{aligned} \tag{S25}$$

Conserved Quantities:

$$G_{tot} = y_1 + y_2 + y_4$$

$$L_{tot} = y_7 + y_8$$

C10: Supremum Model, $N = 10$

$$\begin{aligned}
\dot{y}_2 &= \frac{y_4 (\tilde{y}_6 - c_{fAL} y_5 y_8)}{k_{GA} + y_4 + y_5} \\
\dot{y}_3 &= S - c_{fC} y_3 y_2 \\
\dot{y}_4 &= -\frac{y_4 (\tilde{y}_6 - c_{fAL} y_5 y_8)}{k_{GA} + y_4 + y_5} \\
\dot{y}_5 &= -\frac{y_4 (\tilde{y}_6 - c_{fAL} y_5 y_8)}{k_{GA} + y_4 + y_5} + \tilde{y}_6 - c_{fAL} y_5 y_8 \\
\dot{\tilde{y}}_6 &= -1/\tau_{Am} \tilde{y}_6 + [c_{tsA} \cdot c_{tLA}] y_3^2 + [SA \cdot c_{tLA}] f_U(t) \\
\dot{y}_7 &= c_{fAL} y_5 y_8 - \nu y_7 \\
\dot{y}_8 &= -c_{fAL} y_5 y_8 + \nu y_7 + f_W(t)
\end{aligned} \tag{S26}$$

Conserved Quantities:

$$G_{tot} = y_2 + y_4$$

$$L_{tot} = y_7 + y_8$$

Tables S1-S4 show the limits for the various sequences of reductions, illustrated by the colored arrows in Fig. 3a. As mentioned in the text, given the correct parameterization, each limit can be described by taking a single parameter to zero. These reparameterized parameters are shown in Table S2 for the common limits that are used in the construction of the supremum, indicated by the blue arrow in Fig. 3a. Table S5 shows the original and reparameterized limits side by side.

Red	Green
$c_{tSA} \rightarrow 0$	$SA \rightarrow 0$

TABLE S1. Sequence of limits represented by the red and green arrows in Fig. 3.

Blue	Reparameterized Blue
$c_{bC} \rightarrow 0$	$c_{bC} \rightarrow 0$
$\alpha \rightarrow \infty$	$\frac{1}{\alpha} \rightarrow 0$
$c_{tIA} \rightarrow \infty, SA \rightarrow 0$ (Accumulation) $c_{tIA} \rightarrow \infty, c_{tsA} \rightarrow 0$ (Oscillation) $c_{tIA} \rightarrow \infty, SA \rightarrow 0, c_{tsA} \rightarrow 0$ (Interrupted)	$\frac{1}{c_{tIA}} \rightarrow 0$
$c_{bAL} \rightarrow 0$	$c_{bAL} \rightarrow 0$
$c_{bGA} \rightarrow \infty$ $c_{fGA} \rightarrow \infty$	$\frac{1}{c_{fGA}} \rightarrow 0$

TABLE S2. Sequence of limits represented by the blue arrow in Fig. 3. The second column shows the limits with renormalized parameters such that each limit is given by a single parameter going to zero.

Orange
$SA \cdot c_{tIA} \rightarrow 0$ $\tau_{Am} \rightarrow \infty$
$\frac{c_{bGA}}{c_{fGA}} \rightarrow \infty$ $G_{tot} \rightarrow \infty$
$\frac{G_{tot} \cdot c_{fGA}}{c_{bGA}} \rightarrow \infty$ $c_{fAL} \rightarrow \infty$
$SA \cdot c_{tIA} \cdot \tau_{Am} \rightarrow \infty$ $\frac{G_{tot} \cdot c_{fGA}}{c_{bGA} \cdot c_{fAL}} \rightarrow 0$ $L_{tot} \rightarrow \infty$
$c_{fC} \rightarrow 0$ $\frac{G_{tot} \cdot c_{fGA} \cdot SA \cdot c_{tIA} \cdot \tau_{Am}}{c_{bGA} \cdot c_{fAL}} \rightarrow \infty$ $\nu \rightarrow \infty$
$\frac{G_{tot} \cdot c_{fGA} \cdot SA \cdot c_{tIA} \cdot \tau_{Am}}{c_{bGA} \cdot c_{fAL} \cdot \nu} \rightarrow 0$

TABLE S3. Sequence of limits represented by the orange arrow in Fig. 3.

Black
$c_{bC} \rightarrow 0$
$c_{tLA} \rightarrow \infty$ $SA \rightarrow 0$
$c_{tLA} \cdot SA \rightarrow 0$ $\tau_{Am} \rightarrow \infty$
$c_{bAL} \rightarrow 0$
$c_{fGA} \rightarrow 0$ $G_{tot} \rightarrow \infty$
$\frac{c_{fGA}}{G_{tot}} \rightarrow \infty$ $c_{fAL} \rightarrow \infty$
$\alpha \rightarrow \infty$
$SA \cdot c_{tLA} \cdot \tau_{Am} \rightarrow \infty$ $\frac{G_{tot} \cdot c_{fAL}}{c_{fGA}} \rightarrow \infty$ $L_{tot} \rightarrow \infty$
$c_{bGA} \rightarrow \infty$ $\frac{G_{tot} \cdot c_{fAL}}{c_{fGA} \cdot SA \cdot c_{tLA} \cdot \tau_{Am}} \rightarrow 0$
$c_{fC} \rightarrow 0$ $\frac{G_{tot} \cdot c_{fAL} \cdot c_{bGA}}{c_{fGA} \cdot SA \cdot c_{tLA} \cdot \tau_{Am}} \rightarrow 0$ $\nu \rightarrow \infty$
$\frac{\nu \cdot G_{tot} \cdot c_{fAL} \cdot c_{bGA}}{c_{fGA} \cdot SA \cdot c_{tLA} \cdot \tau_{Am}} \rightarrow \infty$

TABLE S4. Sequence of limits represented by the black arrow in Fig. 3.

Original	Reparameterized
c_{fC}	c_{fC}
c_{bC}	c_{bC}
α	$1/\alpha$
c_{fGA}	$1/c_{fGA}$
c_{bGA}	c_{bGA}/c_{fGA}
S	S
c_{fAL}	c_{fAL}
c_{bAL}	c_{bAL}
c_{tsA}	$[c_{tIA} \cdot c_{tsA}]$
c_{tIA}	$1/c_{tIA}$
τ_{Am}	τ_{Am}
ν	ν
SA	$[c_{tIA} \cdot SA]$
G_{tot}	G_{tot}
L_{tot}	L_{tot}

TABLE S5. Left column: Bare parameters. Right column: Reparameterized parameters used to generate the limits in the right hand column of Table S2.

A. Supremum algorithm – Application to Wnt signaling

The supremum algorithm can be summarized by the following steps:

1. Define the hypothesis space by selecting a complex, multiparameter model to describe the desired behaviors.
2. Find reduced models that minimally describe each behavior.
3. Using the diamond property, and possibly reparameterizing the model, find the approximations common to the both reduced models.
4. Apply those common approximations to the original, full model to obtain the supremal model.

Here we detail this process for the Wnt signaling case from the main text.

The sequence of limits used to arrive at the minimal accumulation model (A3, Eq. S22) are shown in Table S4. To apply the supremum algorithm, the limits that match those used to arrive at the minimal oscillation model (O9, Eq. S21), shown in Table S2, need to be identified. In this case, all of the limits from Table S2 manifest in Table S4. To show this we first needed to reparameterize the model to use the parameters on the right side of Table S5. We applied these limits (from Table S2) to the full model given in Eq S25. Applying these limits gives the supremal model in Eq. S26.

S3. ADDITIONAL SUPREMUM-BUILDING ALGORITHM

The main text presents an algorithm for finding the supremal model: given the parameter limits to arrive at two reduced models, find and apply the common limits to the original full model. We now present a second algorithm that is less straightforward, but equally valid. Given two reduced models, the supremum can be created by taking the union of their relevant mechanisms. It may not be clear how to do this in all cases. However, in the Wnt example this means simply to take the union of the terms in each equations. For example, taking the union of Eqs. S21 and S24 will give Eq. S26. Since the only difference in Eqs. S21 and S24 is in the dynamic variable \tilde{y}_6 we will demonstrate this.

The dynamic equations for \tilde{y}_6 for models A9 and O9 are, respectively,

$$\dot{\tilde{y}}_6 = -1/\tau_{Am}\tilde{y}_6 + [SA \cdot c_{tA}] \quad (\text{S27})$$

$$\dot{\tilde{y}}_6 = -1/\tau_{Am}\tilde{y}_6 + [c_{tsA} \cdot c_{tA}] y_3^2. \quad (\text{S28})$$

Taking the union of terms in these equations gives the dynamic equation for C10, the supremal model

$$\dot{\tilde{y}}_6 = -1/\tau_{Am}\tilde{y}_6 + [c_{tsA} \cdot c_{tA}] y_3^2 + [SA \cdot c_{tA}] f_U(t). \quad (\text{S29})$$

This algorithm can be used when there is a clear connection between the dynamic variables of the reduced models, but it may not be as clear how to apply it otherwise. Additionally, there is no need to know the full model to use this algorithm.

[1] R. Nusse and H. Clevers, Cell **169**, 985 (2017).

- [2] C. Y. Logan and R. Nusse, *Annual Review of Cell and Developmental Biology* **20**, 781 (2004).
- [3] Y. Ding, S. Su, W. Tang, X. Zhang, S. Chen, G. Zhu, J. Liang, W. Wei, Y. Guo, L. Liu, Y.-G. Chen, and W. Wu, *Journal of Cell Science* **127**, 4833 (2014).
- [4] E. Lee, A. Salic, R. Krüger, R. Heinrich, and M. W. Kirschner, *PLOS Biology* **1**, e10 (2003).
- [5] L. Goentoro and M. W. Kirschner, *Molecular Cell* **36**, 872 (2009).
- [6] P. B. Jensen, L. Pedersen, S. Krishna, and M. H. Jensen, *Biophysical Journal* **98**, 943 (2010).